J. Fluid Mech. (1993), *vol.* 250, *pp.* 233–251

Buoyancy effects in stably stratified horizontal boundary-layer flow

By P. G. DANIELS AND R. J. GARGARO
Department of Mathematics, City University, Northampton Square, London, EC1V 0HB, UK

(Received 7 March 1992 and in revised form 7 October 1992)

This paper describes numerical and asymptotic solutions of the steady two-dimensional boundary-layer equations governing buoyant flow on a horizontal, thermally insulated surface. The class of flows considered is one for which there is a uniform external stream at constant temperature but for which conditions upstream lead to a statically stable temperature field within the boundary layer. This has the effect of generating an adverse pressure gradient which, if sufficiently strong, causes the boundary-layer solution to terminate in a singularity. Results are obtained for a range of Prandtl numbers.

1. Introduction

There is a substantial body of work on buoyancy effects in boundary-layer flow. Pohlhausen (1921) proposed the similarity solution for natural convection from a heated vertical plate, and numerical solutions of the governing equations were first obtained by Ostrach (1952). Vertical boundary-layer flows generated by an external stream but for which buoyancy acts to oppose the motion were considered by Merkin (1969) who obtained numerical solutions of the governing partial differential equations and showed how such flows could terminate in a point of separation similar to that associated with a Goldstein (1948) singularity. Buckmaster (1970) and Hunt & Wilks (1980) considered the precise nature of the singularity at separation for isothermal and constant-heat-flux conditions at the wall and further numerical solutions of the boundary-layer equations near separation were also obtained.

Buoyancy effects in horizontal boundary layers appear to have received little attention until the work of Stewartson (1958) who considered natural convection from an isothermal semi-infinite horizontal plate. His results as interpreted by Gill, Zeh & del Casal (1965) established the existence of a similarity solution only for the boundary layer above a heated surface or below a cooled surface, a statically unstable temperature field being necessary to produce a favourable pressure gradient to drive the flow. Theoretical work on the statically stable situation has been carried out using an integral analysis by Clifton & Chapman (1969) while Jones (1973) and Pera & Gebhart (1973) have considered the effect of a small inclination of the plate. Effects of mass transfer from the plate have been considered by Bandrowski & Rybski (1976, see Kerr 1980) and non-Boussinesq effects by Ackroyd (1976). Experimental work on horizontal boundary-layer flow has been reported by Rotem & Claassen (1969), Goldstein, Sparrow & Jones (1973), Al-Arabi and El-Riedy (1976), Faw & Dullforce (1981) and Goldstein & Lau (1983).

For a horizontal boundary layer in which the temperature field is statically stable buoyancy generates an adverse pressure gradient and the flow will break down unless

it is carried forward by the action of an external stream. The balance between these two competing effects is measured by the Froude number of the flow. The aim of the present work is to formulate and solve a model boundary-layer problem for a range of Froude numbers in order to examine the different types of flow that can occur and also ways in which the flow may terminate. In a horizontal buoyancy layer the streamwise pressure gradient varies with depth in the layer and although it is predetermined at the edge of the boundary layer it must otherwise be found as part of the solution process, along with both the temperature and velocity fields. This is different from the situation in a vertical layer where the pressure field is completely predetermined; as a result it is by no means clear that for the horizontal configuration separation can occur in the manner associated with a Goldstein singularity.

The buoyancy-layer problem is formulated in §2 and for a specified class of initial profiles is shown to involve two parameters, the Prandtl number of the fluid, σ, and a second parameter, α, associated with the Froude number of the flow and based on the external flow speed and the heat flux carried by the layer. The initial profiles are chosen to correspond to a non-buoyant wall jet of the type first analysed by Glauert (1956) and for which the corresponding temperature field has been obtained recently by Daniels & Gargaro (1992). This ensures a stable stratification and has the added advantage of providing an initial structure relevant to the intrusion jets observed in certain thermally driven shallow cavity flows. A discussion of this particular application of the work is given in §6. Asymptotic solutions of the horizontal buoyancy-layer system for small and large values of the downstream coordinate are described in §3 and are used as a basis for the construction of a finite-difference numerical scheme in §4. Results of the numerical calculations are described in §5 and a summary of the main conclusions is given in §6.

2. Formulation

Two-dimensional motion in a fluid of mean density ρ, kinematic viscosity ν, thermal diffusivity κ and coefficient of thermal expansion α^* is set up by velocity and temperature profiles of vertical scale $z^* \sim h$ along an insulated horizontal wall which coincides with the x^*-axis. Away from the wall the flow has constant speed U_0^* in the x^*-direction and constant temperature T_0^*. In the Boussinesq approximation the governing equations for steady flow are

$$\frac{\partial \bar{u}}{\partial \bar{x}} + \frac{\partial \bar{w}}{\partial \bar{z}} = 0, \tag{2.1}$$

$$\bar{u}\frac{\partial \bar{u}}{\partial \bar{x}} + \bar{w}\frac{\partial \bar{u}}{\partial \bar{z}} = -\frac{\partial \bar{p}}{\partial \bar{x}} + \nabla^2 \bar{u}, \tag{2.2}$$

$$\bar{u}\frac{\partial \bar{w}}{\partial \bar{x}} + \bar{w}\frac{\partial \bar{w}}{\partial \bar{z}} = -\frac{\partial \bar{p}}{\partial \bar{z}} + \nabla^2 \bar{w} + R\sigma^{-1}\bar{T}, \tag{2.3}$$

$$\bar{u}\frac{\partial \bar{T}}{\partial \bar{x}} + \bar{w}\frac{\partial \bar{T}}{\partial \bar{z}} = \sigma^{-1}\nabla^2 \bar{T}, \tag{2.4}$$

where the velocity components $\bar{u}$, $\bar{w}$ are made non-dimensional by ν/h,

$$(x^*, z^*) = h(\bar{x}, \bar{z})$$

and the pressure and temperature fields are given by

$$p^* = -\rho g^* z^* + (\rho \nu^2/h^2)\,\bar{p}(\bar{x}, \bar{z}), \tag{2.5}$$

$$T^* = T_0^* + T_0^*\,\bar{T}(\bar{x}, \bar{z}), \tag{2.6}$$

where g^* is the acceleration due to gravity which acts in the negative z^*-direction. The two parameters appearing in (2.3) and (2.4) are the Rayleigh number and Prandtl number defined by

$$R = \alpha^* g^* T_0^* h^3/\kappa\nu, \quad \sigma = \nu/\kappa, \tag{2.7}$$

respectively.

In the limit of large Rayleigh number the motion assumes a boundary-layer form in which

$$\bar{T} = T(x,z)+\ldots, \quad \bar{p} = Rp(x,z)+\ldots, \quad \bar{u} = R^{\frac{1}{2}}u(x,z)+\ldots, \quad \bar{w} = w(x,z)+\ldots, \tag{2.8}$$

where $\bar{x} = R^{\frac{1}{2}}x$ and $\bar{z} = z$. Assuming that

$$U_0^* = R^{\frac{1}{2}}U\nu/h \quad (R \gg 1), \tag{2.9}$$

the boundary-layer problem is to solve

$$\frac{\partial u}{\partial x}+\frac{\partial w}{\partial z} = 0, \tag{2.10}$$

$$u\frac{\partial u}{\partial x}+w\frac{\partial u}{\partial z} = -\frac{\partial p}{\partial x}+\frac{\partial^2 u}{\partial z^2}, \tag{2.11}$$

$$0 = -\frac{\partial p}{\partial z}+\sigma^{-1}T, \tag{2.12}$$

$$u\frac{\partial T}{\partial x}+w\frac{\partial T}{\partial z} = \sigma^{-1}\frac{\partial^2 T}{\partial z^2}, \tag{2.13}$$

subject to

$$u = w = \partial T/\partial z = 0 \quad (z = 0), \tag{2.14}$$

$$T \to 0, \quad p \to 0 \quad (z \to \infty), \tag{2.15}$$

and $u \to U$ as $z \to \infty$. A stream function ψ is introduced such that

$$u = \partial\psi/\partial z, \quad w = -\partial\psi/\partial x. \tag{2.16}$$

Initial profiles for T and u are taken to correspond to a non-buoyant wall jet of the type first analysed by Glauert (1956) and characterized by its flux of exterior momentum flux

$$\int_0^\infty u\left(\int_z^\infty u^2\,\mathrm{d}z\right)\mathrm{d}z = P, \tag{2.17}$$

and its heat flux

$$\int_0^\infty \psi\frac{\partial T}{\partial z}\mathrm{d}z = Q. \tag{2.18}$$

The parameters P and Q may in fact be scaled out of the buoyancy-layer problem by means of the transformations

$$\left.\begin{aligned} &x \to PQ^{-\frac{2}{3}}x, \quad z \to P^{\frac{1}{2}}Q^{-\frac{1}{2}}z, \quad T \to P^{-\frac{1}{2}}Q^{\frac{2}{3}}T, \\ &\psi \to P^{\frac{1}{2}}Q^{-\frac{1}{6}}\psi, \quad u \to Q^{\frac{1}{3}}u, \quad w \to P^{-\frac{1}{2}}Q^{\frac{1}{2}}w, \quad p \to Q^{\frac{2}{3}}p, \end{aligned}\right\} \tag{2.19}$$

in which case the governing system is as stated in (2.10)–(2.15) and in addition

$$u \to U/Q^{\frac{1}{3}} \equiv \alpha \quad (z \to \infty). \tag{2.20}$$

The initial jet profile is given by

$$\psi \sim x^{\frac{1}{4}}\phi_0(\mu), \quad T \sim x^{-\frac{1}{4}}\theta_0(\mu) \tag{2.21}$$

as $x \to 0$, where $\mu = z/x^{\frac{3}{4}}$. Here ϕ_0 satisfies

$$\phi_0''' + \tfrac{1}{4}\phi_0\phi_0'' + \tfrac{1}{2}\phi_0'^2 = 0, \tag{2.22}$$

$$\phi_0 = \phi_0' = 0 \quad (\mu = 0), \quad \phi_0' \to 0 \quad (\mu \to \infty), \tag{2.23}$$

and from (2.17) is uniquely defined by the condition

$$\int_0^\infty \phi_0' \left(\int_\mu^\infty \phi_0'^2 \, \mathrm{d}\mu \right) \mathrm{d}\mu = 1, \tag{2.24}$$

while θ_0 satisfies

$$\theta_0'' + \tfrac{1}{4}\sigma(\phi_0'\theta_0 + \phi_0\theta_0') = 0, \tag{2.25}$$

$$\theta_0' = 0 \quad (\mu = 0), \quad \theta_0 \to 0 \quad (\mu \to \infty) \tag{2.26}$$

and is uniquely defined by the condition

$$\int_0^\infty \phi_0 \theta_0' \, \mathrm{d}\mu = 1. \tag{2.27}$$

Since the wall $z = 0$ is thermally insulated and no heat can escape at the edge of the buoyancy layer, integration of the energy equation (2.13) shows that the heat flux in the layer is conserved and is therefore given by the initial value (2.27). Thus

$$\int_0^\infty \psi \frac{\partial T}{\partial z} \mathrm{d}z = 1, \tag{2.28}$$

for all values of x.

The buoyancy-layer problem is seen to depend on two parameters, the Prandtl number σ and the scaled external flow speed α. In fact $\alpha^{\frac{3}{2}} = U^{\frac{3}{2}}/Q^{\frac{1}{2}}$ is associated with the Froude number of the flow (see §6) and is a measure of the size of the forward momentum produced by the external flow relative to the adverse pressure gradient induced by buoyancy.

3. Asymptotic solutions

As the buoyancy-layer flow proceeds downstream the wall jet (2.21) is modified firstly by the presence of the external stream and secondly by the adverse pressure gradient induced by buoyancy. These effects can be seen in an asymptotic expansion of the solution for small values of x, which proceeds initially in powers of $x^{\frac{1}{2}}$:

$$\psi = x^{\frac{1}{4}}\phi_0(\mu) + x^{\frac{3}{4}}\phi_1(\mu) + x^{\frac{5}{4}}\phi_2(\mu) + x^{\frac{7}{4}}\phi_3(\mu) + \ldots, \tag{3.1}$$

$$T = x^{-\frac{1}{4}}\theta_0(\mu) + x^{\frac{1}{4}}\theta_1(\mu) + x^{\frac{3}{4}}\theta_2(\mu) + x^{\frac{5}{4}}\theta_3(\mu) + \ldots, \tag{3.2}$$

$$p = x^{\frac{1}{2}}p_0(\mu) + \ldots. \tag{3.3}$$

Here $\mu = z/x^{\frac{3}{4}}$ and the leading terms which satisfy (2.22)–(2.27) are given by

$$\phi_0 = (40)^{\frac{1}{4}}\Phi^2, \tag{3.4}$$

where

$$\tfrac{1}{4}(40)^{\frac{1}{4}}\mu = \ln \frac{(1 + \Phi + \Phi^2)^{\frac{1}{2}}}{1 - \Phi} + \sqrt{3} \tan^{-1} \frac{\sqrt{3}\Phi}{2 + \Phi} \tag{3.5}$$

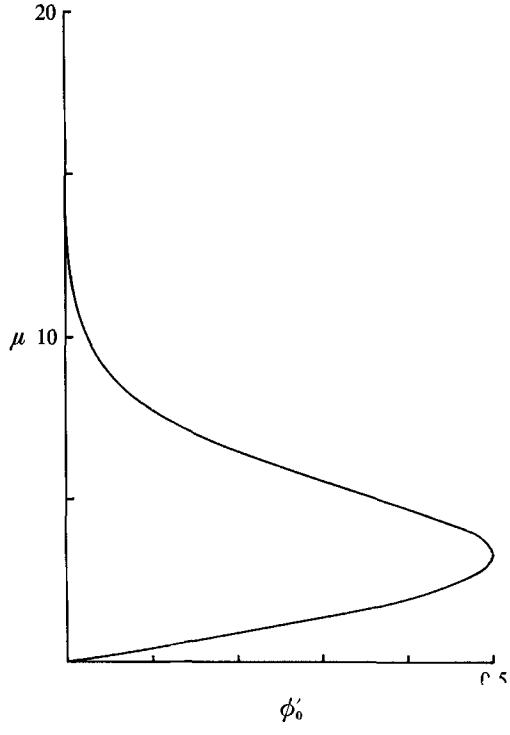

FIGURE 1. The function ϕ_0'.

(Glauert 1956) and
$$\theta_0 = -a_0(1-\Phi^3)^\sigma, \tag{3.6}$$
where
$$a_0 = \Gamma(\sigma+\tfrac{5}{3})/\{\Gamma(\sigma)\,\Gamma(\tfrac{5}{3})\,\sigma(40)^{\frac{1}{4}}\} \tag{3.7}$$
(Daniels & Gargaro 1992).

At first order substitution of (3.1), (3.2) into (2.11)–(2.15), (2.20) shows that ϕ_1 satisfies
$$\phi_1''' + \tfrac{1}{4}\phi_0\phi_1'' + \tfrac{1}{2}\phi_0'\phi_1' + \tfrac{3}{4}\phi_0''\phi_1 = 0, \tag{3.8}$$
$$\phi_1 = \phi_1' = 0 \quad (\mu = 0), \quad \phi_1' \to \alpha \quad (\mu \to \infty), \tag{3.9}$$
and θ_1 satisfies
$$\theta_1'' + \tfrac{1}{4}\sigma(\phi_0\theta_1' - \phi_0'\theta_1) = -\tfrac{1}{4}\sigma(3\phi_1\theta_0' + \phi_1'\theta_0), \tag{3.10}$$
$$\theta_1' = 0 \quad (\mu = 0), \quad \theta_1 \to 0 \quad (\mu \to \infty). \tag{3.11}$$

Similarly, at second order it is found that
$$\phi_2''' + \tfrac{1}{4}\phi_0\phi_2'' + \tfrac{5}{4}\phi_0''\phi_2 = -\tfrac{3}{4}\phi_1\phi_1'', \tag{3.12}$$
$$\phi_2 = \phi_2' = 0 \quad (\mu = 0), \quad \phi_2' \to 0 \quad (\mu \to \infty), \tag{3.13}$$
and
$$\theta_2'' + \tfrac{1}{4}\sigma(\phi_0\theta_2' - 3\phi_0'\theta_2) = \tfrac{1}{4}\sigma(\phi_1'\theta_1 - 3\phi_1\theta_1' - \phi_2'\theta_0 - 5\phi_2\theta_0'), \tag{3.14}$$
$$\theta_2' = 0 \quad (\mu = 0), \quad \theta_2 \to 0 \quad (\mu \to \infty). \tag{3.15}$$

At third order the pressure gradient induced by buoyancy comes into play and ϕ_3 and θ_3 are found to satisfy
$$\phi_3''' + \tfrac{1}{4}\phi_0\phi_3'' - \tfrac{1}{2}\phi_0'\phi_3' + \tfrac{7}{4}\phi_0''\phi_3 = \tfrac{1}{2}p_0 - \tfrac{3}{4}\mu p_0' + \tfrac{1}{2}\phi_1'\phi_2' - \tfrac{3}{4}\phi_1\phi_2'' - \tfrac{5}{4}\phi_1''\phi_2, \tag{3.16}$$
$$\phi_3 = \phi_3' = 0 \quad (\mu = 0), \quad \phi_3' \to 0 \quad (\mu \to \infty), \tag{3.17}$$

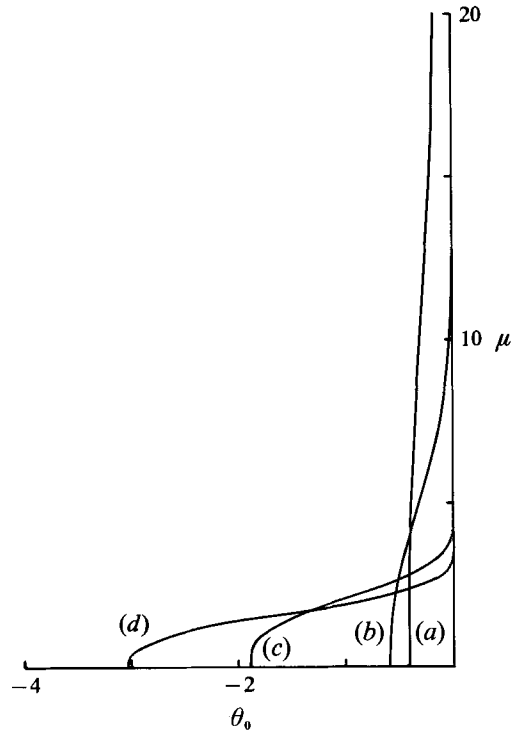

FIGURE 2. The function θ_0 for Prandtl numbers (*a*) 0.1, (*b*) 0.72, (*c*) 8.1, (*d*) 17.2.

where
$$p_0 = -\sigma^{-1}\int_{\mu}^{\infty} \theta_0 \, \mathrm{d}\mu, \tag{3.18}$$

and
$$\theta_3'' + \tfrac{1}{4}\sigma(\phi_0\theta_3' - 5\phi_0'\theta_3) = \tfrac{1}{4}\sigma(3\phi_1'\theta_2 - 3\phi_1\theta_2' + \phi_2'\theta_1 - 5\phi_2\theta_1' - \phi_3'\theta_0 - 7\phi_3\theta_0'), \tag{3.19}$$

$$\theta_3' = 0 \quad (\mu = 0), \quad \theta_3 \to 0 \quad (\mu \to \infty). \tag{3.20}$$

Solutions for ϕ_i and θ_i $(i = 1, 2, 3)$ are found for general values of α by writing

$$\left.\begin{aligned} \phi_1 &= \alpha\tilde{\phi}_1, \quad \phi_2 = \alpha^2\tilde{\phi}_2, \quad \phi_3 = \alpha^3\tilde{\phi}_3 + \bar{\phi}_3, \\ \theta_1 &= \alpha\tilde{\theta}_1, \quad \theta_2 = \alpha^2\tilde{\theta}_2, \quad \theta_3 = \alpha^3\tilde{\theta}_3 + \bar{\theta}_3, \end{aligned}\right\} \tag{3.21}$$

and then the relevant systems for $\tilde{\phi}_i, \tilde{\theta}_i$ and $\bar{\phi}_3, \bar{\theta}_3$ are independent of α; the systems for $\tilde{\phi}_i$ $(i = 1, 2, 3)$ are also independent of the Prandtl number σ. Numerical solutions were obtained using a fourth-order Runge–Kutta scheme and results are displayed in figures 1–3. At the edge of the layer

$$\tilde{\phi}_1 \sim \mu + \tilde{a}_1, \quad \tilde{\phi}_2 \to \tilde{a}_2, \quad \tilde{\phi}_3 \to \tilde{a}_3, \quad \bar{\phi}_3 \to \bar{a}_3(\sigma) \quad (\mu \to \infty), \tag{3.22}$$

and from the numerical solutions $\tilde{a}_1 = -6.92$, $\tilde{a}_2 = 14.9$, $\tilde{a}_3 = -139$ and

$$\bar{a}_3(0.72) = -17.6, \quad \bar{a}_3(8.1) = -0.01.$$

The results indicate that at small values of x the external stream is of primary significance in modifying the jet flow, and enhances its forward velocity of order $x^{-\frac{1}{2}}$ by a finite amount. Buoyancy induces a weaker flow of order x which is associated with

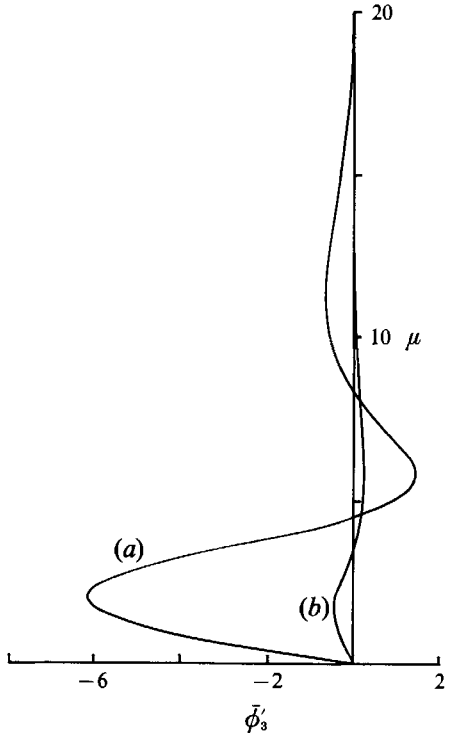

FIGURE 3. The function $\bar{\phi}_3'$ for Prandtl numbers (*a*) 0.72, (*b*) 8.1.

the adverse pressure gradient implied by (3.18) and which is in the upstream direction near the wall (figure 3). In the absence of external flow ($\alpha = 0$) this becomes the major influence on the developing jet and figure 4 gives an impression of the flow development for air predicted by evaluating the expansion (3.1) at finite values of x. Reverse flow first sets in near the edge of the layer and subsequently near the wall.

If the motion is sustained to large values of x it is expected to consist of an externally driven flow modified by buoyancy associated with the temperature field as it relaxes to the uniform value $T = 0$. This suggests an asymptotic form similar to that for a Blasius boundary layer as discussed by Schneider (1979) in which

$$\psi \sim x^{\frac{1}{2}} f(\eta), \quad T \sim x^{-\frac{1}{2}} g(\eta), \quad p \sim q(\eta) \quad (x \to \infty), \tag{3.23}$$

where $\eta = z/x^{\frac{1}{2}}$ and the temperature dependence is dictated by the heat-flux requirement (2.28). Substitution of (3.23) into (2.11)–(2.13) yields

$$f''' + \tfrac{1}{2} f f'' = -\tfrac{1}{2}\eta q', \tag{3.24}$$

$$q' = \sigma^{-1} g, \tag{3.25}$$

$$g'' + \tfrac{1}{2}\sigma(fg' + f'g) = 0, \tag{3.26}$$

and from (2.14), (2.15) and (2.20) the boundary conditions are

$$f = f' = g' = 0 \quad (\eta = 0), \tag{3.27}$$

$$f' \to \alpha, \quad g \to 0, \quad q \to 0 \quad (\eta \to \infty). \tag{3.28}$$

Thus

$$q = -\sigma^{-1} \int_{\eta}^{\infty} g \, \mathrm{d}\eta \tag{3.29}$$

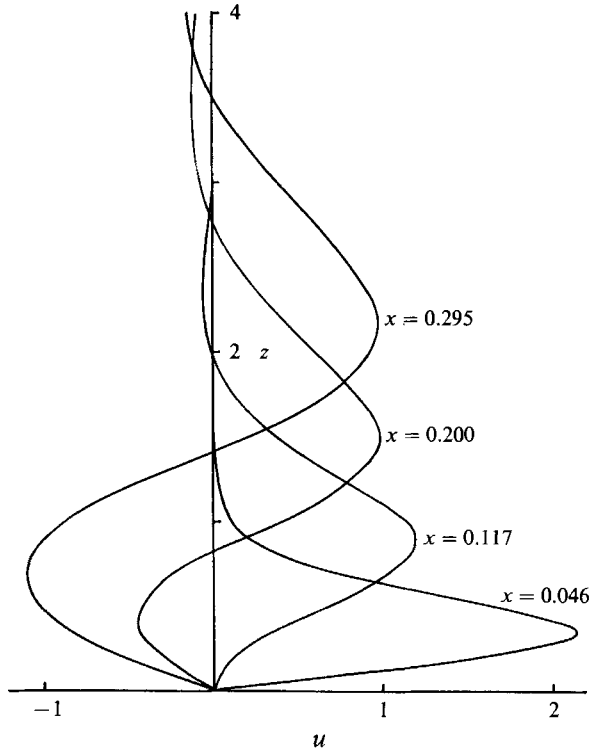

FIGURE 4. $u \sim x^{-\frac{1}{5}}\phi_0' + x\phi_3'$ as a function of z for increasing values of x and $\sigma = 0.72$.

and integration of (3.26) gives

$$g = -\Omega \exp\left(-\tfrac{1}{2}\sigma \int_0^\eta f \, \mathrm{d}\eta\right), \tag{3.30}$$

where Ω is a constant. Substitution into (3.24) and use of the transformation

$$f = \Omega^{\frac{1}{5}} \tilde{f}(\tilde{\eta}), \quad \eta = \Omega^{-\frac{1}{5}} \tilde{\eta}, \tag{3.31}$$

then gives a single equation for $\tilde{f}$:

$$\tilde{f}''' + \tfrac{1}{2}\tilde{f}\tilde{f}'' = \tfrac{1}{2}\tilde{\eta}\sigma^{-1} \exp\left(-\tfrac{1}{2}\sigma \int_0^{\tilde{\eta}} \tilde{f} \, \mathrm{d}\tilde{\eta}\right), \tag{3.32}$$

where the right-hand side represents the adverse pressure gradient induced by buoyancy. This equation must be solved subject to

$$\tilde{f} = \tilde{f}' = 0 \quad (\tilde{\eta} = 0), \quad \tilde{f}' \to \tilde{\alpha} \quad (\tilde{\eta} \to \infty), \tag{3.33}$$

where

$$\tilde{\alpha} = \Omega^{-\frac{2}{5}} \alpha. \tag{3.34}$$

The integral constraint (2.28) requires that

$$\int_0^\infty f g' \, \mathrm{d}\eta = 1, \tag{3.35}$$

and so gives

$$\Omega^{\frac{6}{5}} I = 1, \tag{3.36}$$

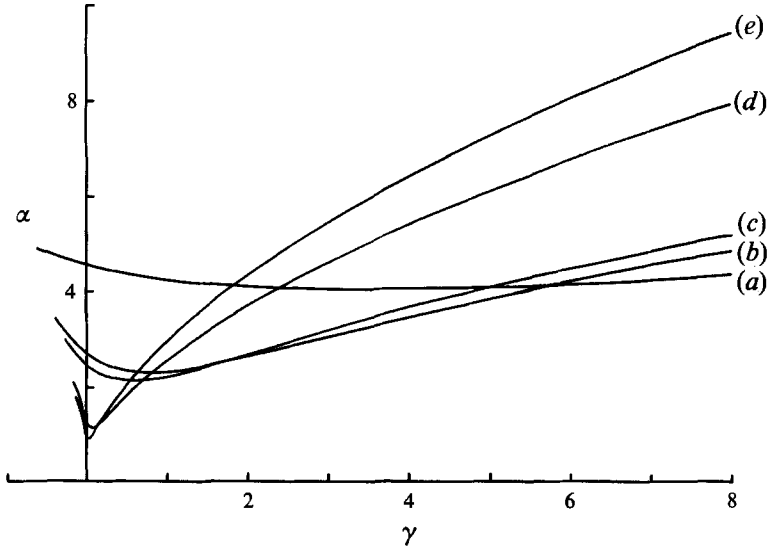

FIGURE 5. The parameter α as a function of γ for Prandtl numbers (*a*) 0.1, (*b*) 0.72, (*c*) 1.0, (*d*) 8.1, (*e*) 17.2.

γ	Ω	α	$q(0)$	$-(\tilde{f}-\tilde{\alpha}\tilde{\eta})_\infty$
0.0	0.3817	2.683	2.079	10.53
0.5	0.4092	2.325	1.747	6.499
1.0	0.3910	2.333	1.448	5.116
1.5	0.3688	2.476	1.239	4.594
2.0	0.3493	2.665	1.091	4.399
2.5	0.3330	2.869	0.981	4.347
3.0	0.3193	3.075	0.896	4.364
3.5	0.3076	3.280	0.829	4.417
4.0	0.2976	3.479	0.773	4.489
4.5	0.2889	3.673	0.727	4.571
5.0	0.2812	3.862	0.688	4.658
5.5	0.2743	4.046	0.654	4.748
6.0	0.2681	4.224	0.624	4.839
10.0	0.2338	5.502	0.473	5.519
15.0	0.2092	6.842	0.378	6.225
20.0	0.1933	8.004	0.323	6.811
25.0	0.1818	9.047	0.285	7.315
30.0	0.1728	10.003	0.258	7.760

TABLE 1. Properties of the large-x asymptote for $\sigma = 0.72$

where
$$I = \tfrac{1}{2}\sigma \int_0^\infty \tilde{f}^2 \exp\left(-\tfrac{1}{2}\sigma \int_0^{\tilde{\eta}} \tilde{f}\,\mathrm{d}\tilde{\eta}\right)\mathrm{d}\tilde{\eta}. \tag{3.37}$$

Solutions of (3.32) were computed by specifying $\gamma = \tilde{f}''(0)$ and integrating outwards by a fourth-order Runge–Kutta scheme to obtain $\tilde{\alpha} = \tilde{f}'(\infty)$. Then α may be calculated retroactively from (3.34) and (3.36) as

$$\alpha = \tilde{\alpha} I^{-\frac{1}{3}}. \tag{3.38}$$

Computations of α as a function of γ for a range of Prandtl numbers are shown in figure 5. This shows that such solutions only exist for values of α in the range $\alpha > \alpha_c(\sigma)$ and that for a given α in this range there are dual solutions for f. Some of these

solutions exhibit reverse flow near the wall. Table 1 gives values of Ω and α for various values of γ, as well as the quantities $q(0)$ and $(\tilde{f}-\tilde{\alpha}\tilde{\eta})_\infty$ which are needed in order to determine the wall pressure and displacement thickness of the boundary layer (see (5.2), (5.9) below).

Further terms in the asymptotic forms (3.23) have not been considered in detail although there are certainly terms of relative order x^{-1} equivalent to a shift in origin of the expansion.

4. Numerical solution

Full numerical solutions of the buoyancy-layer system (2.10)–(2.15) and (2.20) were obtained using a finite-difference scheme. The system is parabolic and solutions were computed by a downstream marching procedure, using Newton iteration to solve the discretized form of the nonlinear equations at each x-station. In view of the initial development outlined in §3, in $x < 1$ the equations were discretized onto a mesh which conformed with the asymptotic structure as $x \to 0$. Thus the solution is written as

$$\psi = \xi A(\xi,\mu), \quad p = \sigma^{-1}\xi^2 D(\xi,\mu), \quad T = \xi^{-1}E(\xi,\mu), \tag{4.1}$$

where

$$\xi = x^{\frac{1}{4}}, \quad \mu = z/x^{\frac{3}{4}}, \tag{4.2}$$

giving equations which may be expressed in first-order form as

$$\frac{\partial C}{\partial \mu} = \tfrac{1}{4}\xi\left(B\frac{\partial B}{\partial \xi} - C\frac{\partial A}{\partial \xi}\right) - \tfrac{1}{2}B^2 - \tfrac{1}{4}AC + \tfrac{1}{4}\sigma^{-1}\xi^6\left(2D + \xi\frac{\partial D}{\partial \xi} - 3\mu E\right), \tag{4.3}$$

$$\frac{\partial F}{\partial \mu} = \tfrac{1}{4}\sigma\left(\xi\left(B\frac{\partial E}{\partial \xi} - F\frac{\partial A}{\partial \xi}\right) - EB - AF\right), \tag{4.4}$$

with

$$B = \frac{\partial A}{\partial \mu}, \quad C = \frac{\partial B}{\partial \mu}, \quad E = \frac{\partial D}{\partial \mu}, \quad F = \frac{\partial E}{\partial \mu}. \tag{4.5}$$

The boundary conditions are

$$A = B = F = 0 \quad (\mu = 0), \tag{4.6}$$

$$D \to 0, \quad E \to 0, \quad B \to \alpha\xi^2 \quad (\mu \to \infty), \tag{4.7}$$

and the initial profiles are

$$A = \phi_0, \quad B = \phi_0', \quad C = \phi_0'', \quad D = \sigma p_0, \quad E = \theta_0, \quad F = \theta_0' \quad (\xi = 0). \tag{4.8}$$

The equations and boundary conditions are discretized using central differences and uniform steps $\Delta\xi$ and $\Delta\mu$. Details of the resulting matrix equation for the Newton increments at each downstream step are given by Gargaro (1991); the solution at the previous step is used to provide an initial guess and convergence is required to within a specified tolerance.

At $x = 1$ a switch is made to a uniform mesh in

$$X = x^{\frac{1}{2}}, \quad \eta = z/x^{\frac{1}{2}}, \tag{4.9}$$

with

$$\psi = X\tilde{A}(X,\eta), \quad p = \sigma^{-1}\tilde{D}(X,\eta), \quad T = X^{-1}\tilde{E}(X,\eta), \tag{4.10}$$

which ensures that the widening layer is adequately resolved in the numerical scheme

ξ	$\Delta\xi = 0.02, \Delta\mu = 0.1$	$\Delta\xi = 0.02, \Delta\mu = 0.2$
0.2	1.0017	1.0017
0.4	1.0014	1.0005
0.6	1.0010	0.9991
0.8	1.0006	0.9975
1.0	0.9998	0.9948

TABLE 2. Values of the conserved integral (2.28) for $\sigma = 0.72$, $\alpha = 10$ and different step sizes

at large values of x, in line with the asymptotic form (3.23). For $x > 1$ the system of first-order equations

$$\frac{\partial \tilde{C}}{\partial \eta} = \tfrac{1}{2}X\left(\tilde{B}\frac{\partial \tilde{B}}{\partial X} - \tilde{C}\frac{\partial \tilde{A}}{\partial X}\right) - \tfrac{1}{2}\tilde{A}\tilde{C} + \tfrac{1}{2}\sigma^{-1}\left(X\frac{\partial \tilde{D}}{\partial X} - \eta\tilde{E}\right), \tag{4.11}$$

$$\frac{\partial \tilde{F}}{\partial \eta} = \tfrac{1}{2}\sigma\left(X\left(\tilde{B}\frac{\partial \tilde{E}}{\partial X} - \tilde{F}\frac{\partial \tilde{A}}{\partial X}\right) - \tilde{B}\tilde{E} - \tilde{A}\tilde{F}\right), \tag{4.12}$$

$$\tilde{B} = \frac{\partial \tilde{A}}{\partial \eta}, \quad \tilde{C} = \frac{\partial \tilde{B}}{\partial \eta}, \quad \tilde{E} = \frac{\partial \tilde{D}}{\partial \eta}, \quad \tilde{F} = \frac{\partial \tilde{E}}{\partial \eta}, \tag{4.13}$$

must be solved subject to the boundary conditions

$$\tilde{A} = \tilde{B} = \tilde{F} = 0 \quad (\eta = 0), \tag{4.14}$$

$$\tilde{D} \to 0, \quad \tilde{E} \to 0, \quad \tilde{B} \to \alpha \quad (\eta \to \infty). \tag{4.15}$$

At the changeover point $x = \xi = X = 1$ the initial profiles for $\tilde{A}, \tilde{B}, \ldots$ are simply given by $A, B, \ldots$. The system is discretized onto a uniform mesh in X and η and Newton iteration again used to obtain the solution at each downstream step. Details are given by Gargaro (1991).

Most computations were performed with step sizes $\Delta\mu = \Delta\eta = 0.1$ and $\Delta\xi = \Delta X = 0.02$ and with 500 steps across the layer. The tolerance for which the Newton increments were considered small enough was usually taken as 10^{-4}. Various checks on accuracy were carried out by using different step sizes and also by computing the conserved integral (2.28) at each downstream step; some of the results are summarized in table 2.

5. Numerical results

The range of α considered was from 0 to 10 and most results were obtained for $\sigma = 0.72$ (air) and $\sigma = 8.1$ (water). At sufficiently low values of α the numerical solution terminated either because of the onset of reverse flow or because a singularity was reached at a finite value of x. Reverse-flow breakdown occurred for $\sigma = 0.72$ and $\alpha = 0$. The asymptotic theory of § 3 suggested that reverse flow might first occur towards the edge of the layer and this was indeed the case, leading to the failure of the numerical computation just beyond $\xi = 0.32$.

Breakdown in the form of a singularity was observed for higher values of α. The case investigated in detail was $\alpha = 1$, $\sigma = 0.72$. The flow appeared to be developing in a regular manner, but broke down quickly as the singularity was approached at $\xi \approx 0.5336$. Near to the singularity the pressure gradient became favourable and the skin friction increased rapidly. The same type of singularity occurred for $\sigma = 0.72$ and

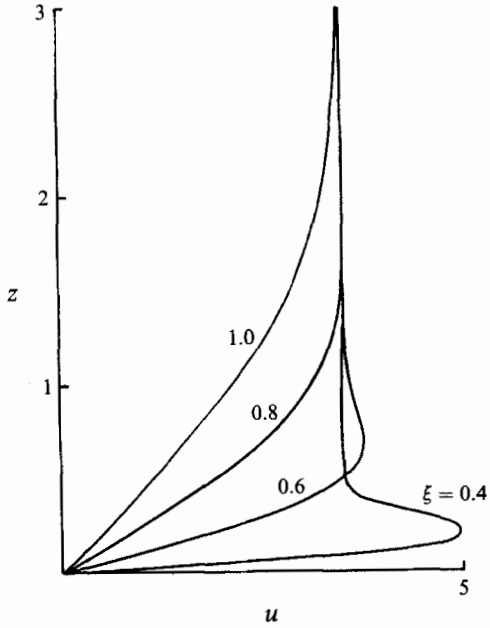

FIGURE 6. Velocity profiles for $\sigma = 0.72$, $\alpha = 3.5$ and $\xi = 0.4, 0.6, 0.8, 1.0$.

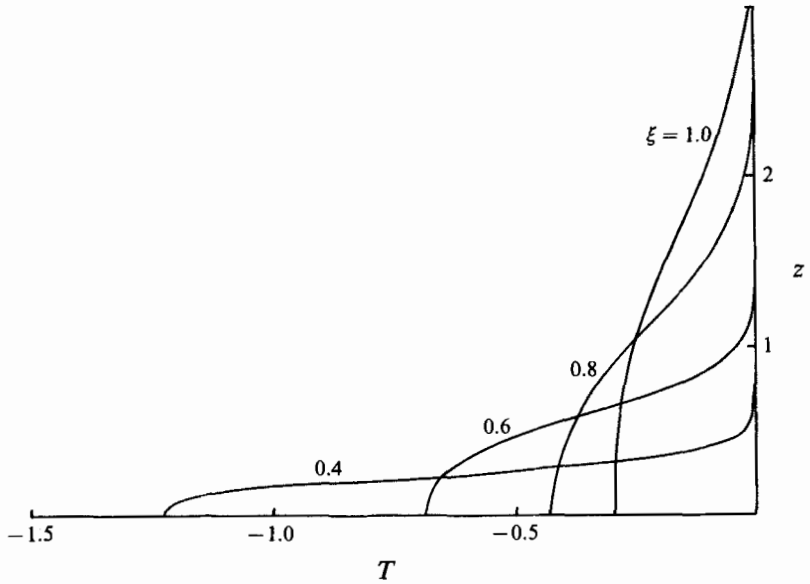

FIGURE 7. Temperature profiles for $\sigma = 0.72$, $\alpha = 3.5$ and $\xi = 0.4, 0.6, 0.8, 1.0$.

$\alpha = 2, 3$ and 3.5, the terminal point of the boundary layer extending further downstream as α increased. For $\alpha = 3.5$ the singularity occurred between $x = 10$ and 10.5. When the value of α was raised to 4 or more the flow was able to develop fully downstream to the asymptote associated with the right-hand branch of figure 5. Typical graphs of velocity, temperature and pressure are shown in figures 6, 7 and 8.

At higher Prandtl number ($\sigma = 8.1$) the terminal singularity was confined to a smaller range of α and for $\alpha = 3$ the flow was able to develop all the way along the

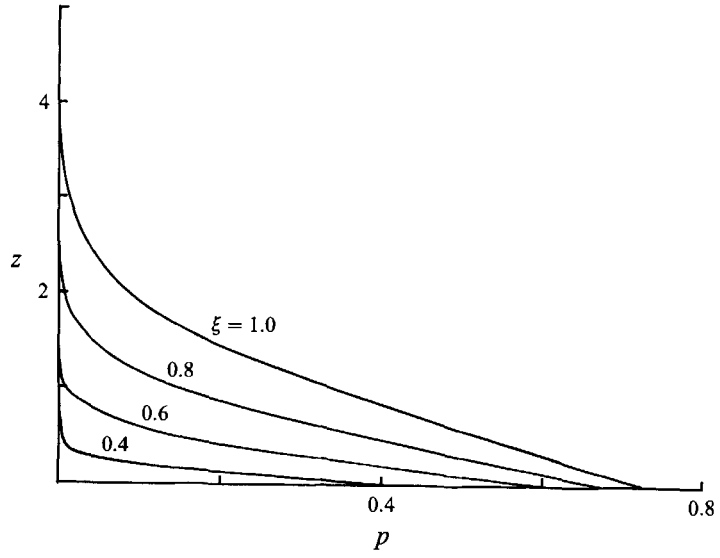

FIGURE 8. Pressure profiles for $\sigma = 0.72$, $\alpha = 3.5$ and $\xi = 0.4, 0.6, 0.8, 1.0$.

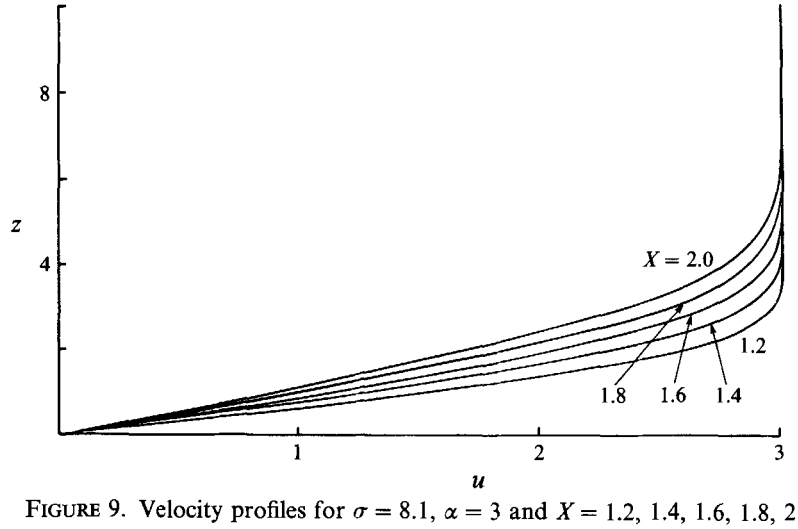

FIGURE 9. Velocity profiles for $\sigma = 8.1$, $\alpha = 3$ and $X = 1.2, 1.4, 1.6, 1.8, 2.0$.

boundary layer. Graphs of velocity and temperature in figures 9 and 10 illustrate the evolution of the jet into the new flow structure in which buoyancy and the forcing external velocity are in balance.

The downstream development of the buoyancy layer for the case of air is summarized in figures 11–14. Figure 11 shows the wall pressure plotted against ξ for various α, for which the asymptotic behaviour predicted in §3 is

$$p(x,0) \sim x^{\frac{1}{2}} a_0 \, \Gamma(\tfrac{1}{3}) \Gamma(\sigma)/\{\sigma \Gamma(\tfrac{1}{3}+\sigma)\} \quad (x \to 0), \tag{5.1}$$

$$p(x,0) \to q(0) \quad (x \to \infty). \tag{5.2}$$

The cases $\alpha = 4$ and 10 which develop all the way along the boundary layer do approach the relevant asymptotes and even those cases which terminate but for which

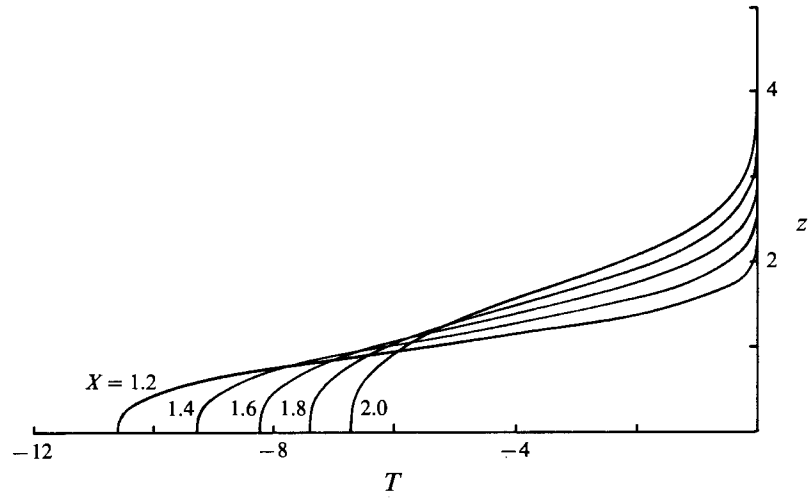

FIGURE 10. Temperature profiles for $\sigma = 8.1$, $\alpha = 3$ and $X = 1.2$, 1.4, 1.6, 1.8, 2.0.

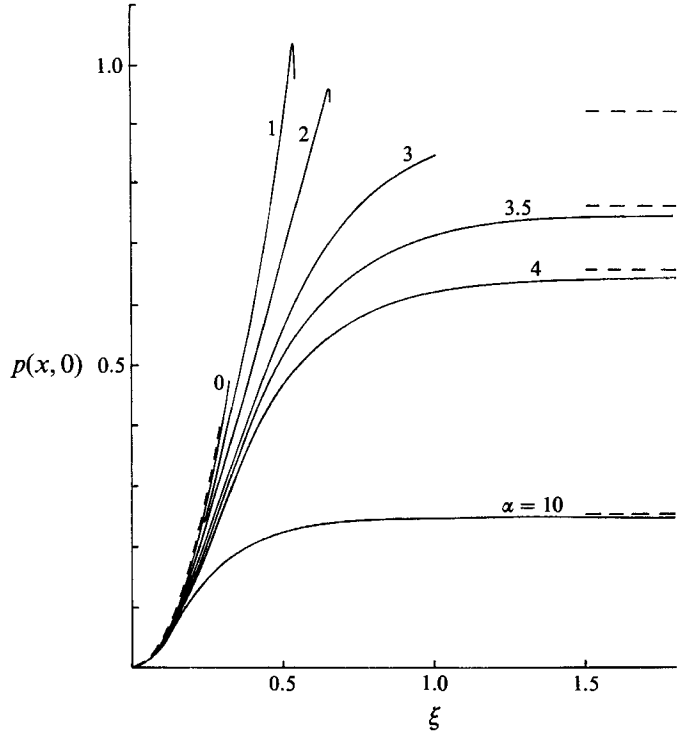

FIGURE 11. Wall pressure for $\sigma = 0.72$ and various values of α. Dashed curves show the asymptotes (5.1), (5.2).

$\alpha > \alpha_c(0.72) \approx 2.3$ actually appear to approach their large-x asymptotes prior to termination. Detailed computations were carried out close to the singularity for the two cases $\alpha = 1$ and 2 to reveal the local behaviour shown in figure 11.

Asymptotic forms for the skin friction and wall temperature at small and large values of x are

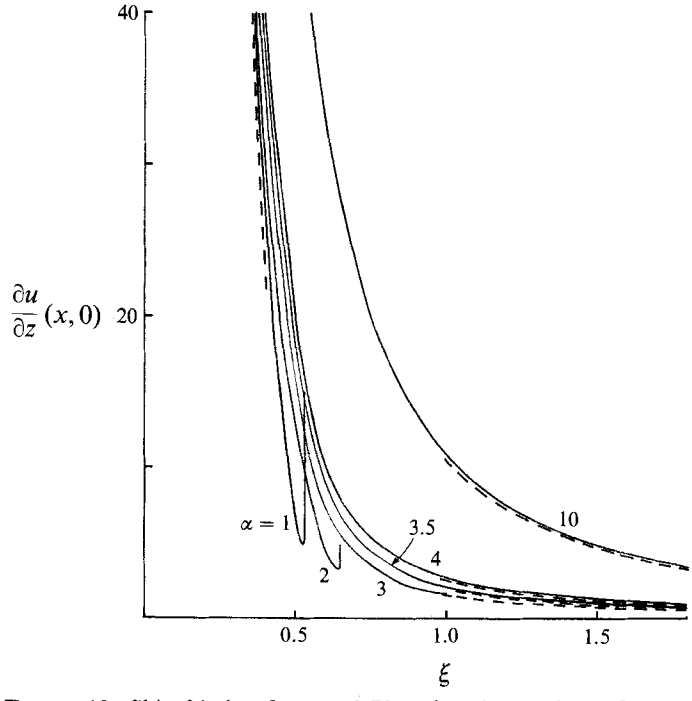

FIGURE 12. Skin friction for $\sigma = 0.72$ and various values of α. Dashed curves show the asymptotes (5.3), (5.4).

$$(\partial u/\partial z)(x,0) \sim x^{-\frac{5}{4}}(40)^{\frac{3}{4}}/72 \quad (x \to 0), \tag{5.3}$$

$$(\partial u/\partial z)(x,0) \sim x^{-\frac{1}{2}}\Omega^{\frac{3}{5}}\gamma \quad (x \to \infty), \tag{5.4}$$

$$T(x,0) \sim -x^{-\frac{1}{4}}a_0 \quad (x \to 0), \tag{5.5}$$

$$T(x,0) \sim -x^{-\frac{1}{2}}\Omega \quad (x \to \infty), \tag{5.6}$$

and these are included in figures 12 and 13. The cases $\alpha = 1$ and 2 indicate that the skin friction increases without bound as the singularity is approached while the wall temperature is relatively little affected.

The displacement $d(x)$ is defined by the outer behaviour

$$\psi \sim \alpha z - d(x) \quad (z \to \infty), \tag{5.7}$$

and is shown in figure 14. Its asymptotes for small and large values of x are

$$d(x) \sim -x^{\frac{1}{4}}(40)^{\frac{1}{4}} \quad (x \to 0), \tag{5.8}$$

$$d(x) \sim -x^{\frac{1}{2}}\Omega^{\frac{1}{5}}(\tilde{f} - \tilde{\alpha}\tilde{\eta})_\infty \quad (x \to \infty), \tag{5.9}$$

and again there is good agreement with the computations. For $\alpha = 1$ and 2 the displacement turns sharply downwards as the singularity is approached, indicating that fluid is being brought back down into the boundary layer.

Quantitative comparisons of the computations with the complete small-x expansions of §3 were found to be satisfactory and details are given by Gargaro (1991). It should be noted that the asymptotic expansions require both $x^{\frac{1}{2}}$ and $\alpha x^{\frac{1}{2}}$ to be small compared with unity and the latter condition implies an increasingly severe limitation on the range of x for validity of the expansion at high values of α.

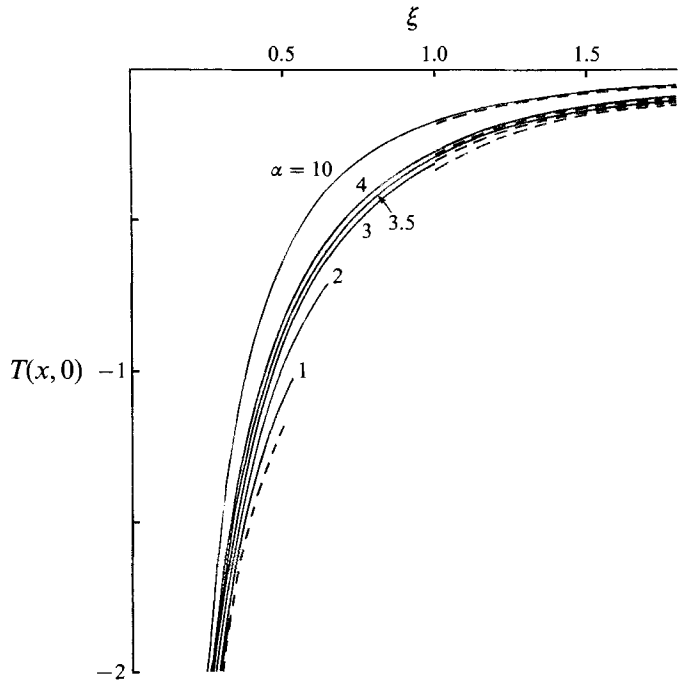

FIGURE 13. Wall temperature for $\sigma = 0.72$ and various values of α. Dashed curves show the asymptotes (5.5), (5.6).

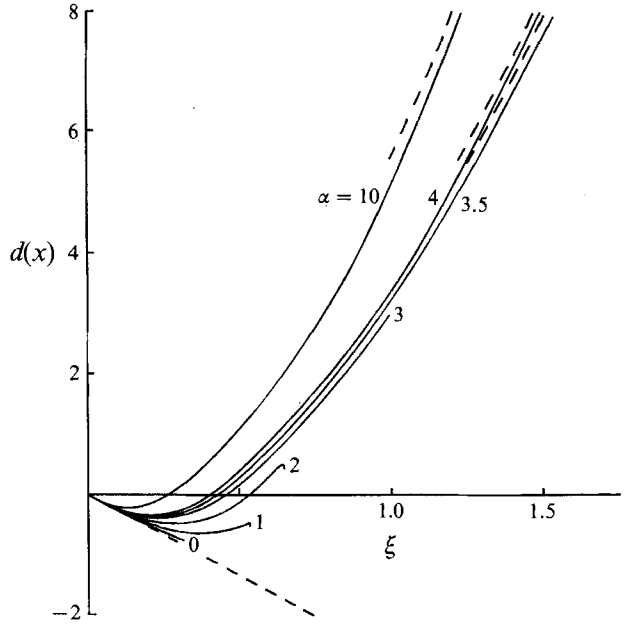

FIGURE 14. Displacement for $\sigma = 0.72$ and various values of α. Dashed curves show the asymptotes (5.8), (5.9).

6. Summary and discussion

A model boundary-layer problem in which buoyancy plays a significant role has been formulated for flow along a horizontal, thermally insulated wall. For the situation in which the boundary layer is initiated by a non-buoyant wall jet the solution is dependent on only two parameters, the Prandtl number of the fluid σ and α, as defined by (2.20). A useful interpretation of the parameter α is obtained by considering the Froude number of the flow. A local Froude number in the boundary layer is based on the ratio of inertia to buoyancy

$$u^*/\{\alpha^* g^*(T_0^* - T^*)\, z^*\}^{\frac{1}{2}}, \tag{6.1}$$

where u^* is the streamwise velocity in the boundary layer. It is readily established from (3.1), (3.2) that this is large (of order $x^{-\frac{3}{4}}$) in the jet flow upstream, where inertia is dominant. As the jet diffuses, buoyancy comes into play and the local Froude number decreases. A global Froude number, on the other hand, can be defined in terms of the external flow U_0^* as

$$Fr = U_0^{*\frac{3}{2}} \Big/ \left\{\alpha^* g^* \int_0^\infty u^*(T_0^* - T^*)\, \mathrm{d}z^*\right\}^{\frac{1}{2}}, \tag{6.2}$$

and this is directly related to the parameter α by the formula

$$Fr = \sigma^{\frac{1}{2}} \alpha^{\frac{3}{2}}. \tag{6.3}$$

In cases where the Froude number is too low the boundary-layer flow cannot be sustained and the forward motion succumbs to the adverse pressure gradient induced by buoyancy. This either leads to the onset of reverse flow and the consequent failure of the numerical scheme or more generally to the occurrence of a terminal singularity. In cases where reverse flow sets in, the computations failed due to numerical instability rather than the existence of any local singular behaviour. The flow becomes subject to upstream influence which requires a much more sophisticated numerical treatment beyond the scope of the present work. In the case of the terminal singularity, the local Froude number in the boundary layer reaches a critically low level from which the flow is unable to recover on the boundary-layer lengthscale. Locally however the singularity is characterized by an apparent recovery, with a rapidly increasing skin friction and a favourable pressure gradient. Computations very close to the singularity revealed the development of an intricate and clearly defined structure in which the streamwise pressure gradient, skin friction and streamwise temperature gradient all become infinitely large as x approaches a finite station within the boundary layer. The boundary-layer solution cannot proceed at this point. A local analysis which takes into account streamwise gradients not included in the boundary-layer model is required to determine whether the singularity heralds a complete breakdown of the theory, analogous to that of the Goldstein (1948) singularity in classical pressure-driven boundary layers, or whether the upstream flow can be matched via a local adjustment to a consistent solution downstream. A detailed analysis of the structure of the singularity and a discussion of its possible relevance to the occurrence of internal hydraulic jumps (Turner 1973; Ivey 1984) is given elsewhere (Daniels 1992). None of the computations revealed any kind of flow separation from the wall or a singularity of the type associated with a Goldstein structure although the possibility of other terminal behaviour for more general initial configurations should not be ruled out and has been observed, for example, by Schneider & Wasel (1985).

In general the computations ended in the terminal singularity for a wider range of values of α than the range $\alpha < \alpha_c(\sigma)$ associated with non-existence of an asymptotic

solution at large values of x. Thus for example in the case of air, the singularity occurred for values of α as high as 3.5 whereas the critical value predicted in §3 is $\alpha_c(0.72) \approx 2.3$. For those solutions which do attain the large-x asymptotic form, in which a balance is achieved between the external driving force and buoyancy, there was found to be excellent agreement between the numerical computations and the asymptotic predictions of §3. As the boundary layer proceeds downstream, isotherms stemming from the jet flow at $x = 0$ attach to the wall and the temperature of the wall rises to the ambient temperature of the external flow.

The present work was partially motivated by the desire to understand the properties of horizontal boundary layers in thermal cavity flows. Such flows, driven for example by maintaining the vertical walls of a cavity at different temperatures, exhibit jet-like behaviour in regions at the bottom of the cold wall (and the top of the hot wall) where fluid descending (or ascending) in a vertical boundary layer issues into the core. These intrusion jets (Bejan, Al-Homoud & Imberger 1981; Simpkins & Chen 1986) are stably stratified and in certain flow regimes may also be modified by a recirculating core flow equivalent to the uniform external stream incorporated here. Such a structure has been proposed by Daniels (1993) in connection with thermally driven flow in shallow cavities and the present work is an investigation of the second stage of evolution of the relevant horizontal boundary-layer structure. The first stage consists of a non-buoyant wall jet and has been discussed by Daniels & Gargaro (1992). The consistency of the horizontal layers is an important ingredient in verifying the overall consistency of the high Rayleigh number flow structure in the cavity, as this is primarily dependent on the requirement that heat flux is conveyed from the hot wall to the cold wall via the horizontal boundary layers. The present study indicates that the local Froude number of the flow is a crucial factor in determining whether a self-contained horizontal boundary-layer flow is feasible.

R.J.G. would like to thank the Science and Engineering Research Council for support in the form of a research studentship.

REFERENCES

Ackroyd, J. A. D. 1976 Laminar natural convection boundary layers on near-horizontal plates. *Proc. R. Soc. Lond.* A **352**, 249.

Al-Arabi, M. & El-Riedy, M. K. 1976 Natural convection heat transfer from isothermal horizontal plates of different shapes. *Intl J. Heat Mass Transfer* **19**, 1399.

Bandrowski, J. & Rybski, W. 1976 Free convection mass transfer from horizontal plates. *Intl J. Heat Mass Transfer* **19**, 827.

Bejan, A., Al-Homoud, A. A. & Imberger, J. 1981 Experimental study of high Rayleigh number convection in a horizontal cavity with different end temperatures. *J. Fluid Mech.* **109**, 283.

Buckmaster, J. 1970 The behaviour of a laminar compressible boundary layer on a cold wall near a point of zero skin friction. *J. Fluid Mech.* **44**, 237.

Clifton, J. V. & Chapman, A. J. 1969 Natural convection on a finite-size horizontal plate. *Intl J. Heat Mass Transfer* **12**, 1573.

Daniels, P. G. 1992 A singularity in thermal boundary-layer flow on a horizontal surface. *J. Fluid Mech.* **242**, 419.

Daniels, P. G. 1993 High Rayleigh number thermal convection in a shallow laterally heated cavity. *Proc. R. Soc. Lond.* (to appear).

Daniels, P. G. & Gargaro, R. J. 1992 Numerical and asymptotic solutions for the thermal wall jet. *J. Engng Maths* **26**, 493.

Faw, R. E. & Dullforce, T. A. 1981 Holographic interferometry measurement of convective heat transfer beneath a heated horizontal plate in air. *Intl J. Heat Mass Transfer* **24**, 859.

GARGARO, R. J. 1991 Thermally driven shallow cavity flows. PhD thesis, City University, London.

GILL, W. N., ZEH, D. W. & CASAL, E. DEL 1965 Free convection on a horizontal plate. *Z. Angew Math. Phys.* **16**, 539.

GLAUERT, M. B. 1956 The wall jet. *J. Fluid Mech.* **1**, 625.

GOLDSTEIN, R. J. & LAU, K.-S. 1983 Laminar natural convection from a horizontal plate and the influence of plate-edge extensions. *J. Fluid Mech.* **129**, 55.

GOLDSTEIN, R. J., SPARROW, E. M. & JONES, D. C. 1973 Natural convection mass transfer adjacent to horizontal plates. *Intl J. Heat Mass Transfer* **16**, 1025.

GOLDSTEIN, S. 1948 On laminar boundary layer flow near a position of separation. *Q. J. Mech. Appl. Maths* **1**, 43.

HUNT, R. & WILKS, G. 1980 On the behaviour of the laminar boundary-layer equations of mixed convection near a point of zero skin friction. *J. Fluid Mech.* **101**, 377.

IVEY, G. N. 1984 Experiments on transient natural convection in a cavity. *J. Fluid Mech.* **144**, 389.

JONES, D. R. 1973 Free convection from a semi-infinite flat plate inclined at a small angle to the horizontal. *Q. J. Mech. Appl. Maths* **26**, 77.

KERR, C. N. 1980 Analog solution of free convection mass transfer from downward-facing horizontal plates. *Intl J. Heat Mass Transfer* **23**, 247.

MERKIN, J. 1969 The effect of buoyancy forces on the boundary layer flow over a semi-infinite vertical flat plate in a uniform stream. *J. Fluid Mech.* **35**, 439.

OSTRACH, S. 1952 An analysis of laminar free convection flow and heat transfer about a flat plate parallel to the direction of the generating body force. *NACA Tech. Note* 2635, Washington DC.

PERA, L. & GEBHART, B. 1973 Natural convection boundary layer flow over horizontal and slightly inclined surfaces. *Intl J. Heat Mass Transfer* **16**, 1131.

POHLHAUSEN, E. 1921 Der warmeaustausch zwichen festen korpern und flussigkeiten mit kleiner reibung und warmeleitung. *Z. Angew Math. Mech.* **1**, 115.

ROTEM, Z. & CLAASSEN, L. 1969 Natural convection above unconfined horizontal surfaces. *J. Fluid Mech.* **39**, 173.

SCHNEIDER, W. 1979 A similarity solution for combined forced and free convection. *Intl J. Heat Mass Transfer* **22**, 1401.

SCHNEIDER, W. & WASEL, M. G. 1985 Breakdown of the boundary-layer approximation for mixed convection above a horizontal plate. *Intl J. Heat Mass Transfer* **28**, 2307.

SIMPKINS, P. G. & CHEN, K. S. 1986 Convection in horizontal cavities. *J. Fluid Mech.* **166**, 21.

STEWARTSON, K. 1958 On the free convection from a horizontal plate. *Z. Angew Math. Phys.* **9**, 276.

TURNER, J. S. 1973 *Buoyancy Effects in Fluids.* Cambridge University Press.